THE JOURNAL OF PHYSICAL CHEMISTRY C

Article

Cite This: J. Phys. Chem. C 2018, 122, 17660−17667

pubs.acs.org/JPCC

Stabilizing Lead-Free All-Inorganic Tin Halide Perovskites by Ion Exchange

Junke Jiang,[†] Chidozie K. Onwudinanti,[‡] Ross A. Hatton,[§] Peter A. Bobbert,[†,∥] and Shuxia Tao*[,†]

[†]Center for Computational Energy Research, Department of Applied Physics, and [∥]Molecular Materials and Nano Systems, Department of Applied Physics, Eindhoven University of Technology, P.O. Box 513, 5600 MB Eindhoven, The Netherlands

[‡]Center for Computational Energy Research, DIFFER—Dutch Institute for Fundamental Energy Research, De Zaale 20, 5612 AJ Eindhoven, The Netherlands

[§]Department of Chemistry, University of Warwick, CV4 7AL Coventry, U.K.

Supporting Information

ABSTRACT: Because of its thermal stability, lead-free composition, and nearly ideal optical and electronic properties, the orthorhombic $CsSnI_3$ perovskite is considered promising as a light absorber for lead-free all-inorganic perovskite solar cells. However, the susceptibility of this three-dimensional perovskite toward oxidation in air has limited the development of solar cells based on this material. Here, we report the findings of a computational study which identifies promising $Rb_yCs_{1-y}Sn(Br_xI_{1-x})_3$ perovskites for solar cell applications, prepared by substituting cations (Rb for Cs) and anions (Br for I) in $CsSnI_3$. We show the evolution of the material electronic structure as well as its thermal and structural stabilities upon gradual substitution. Importantly, we demonstrate how the unwanted yellow phase can be suppressed by substituting Br for I in $CsSn(Br_xI_{1-x})_3$ with $x \geq 1/3$. We predict that substitution of Rb for Cs results in a highly homogeneous solid solution and therefore an improved film quality and applicability in solar cell devices.

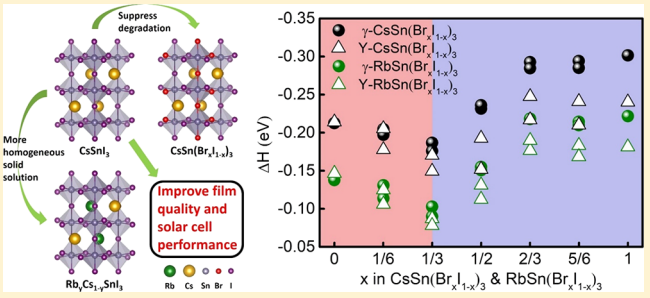

INTRODUCTION

Organic−inorganic hybrid halide perovskite solar cells (PSCs) have attracted strong attention in the past few years and are becoming one of the most promising types of emerging thin-film solar cells.[1−4] In less than a decade, the power conversion efficiency (PCE) of PSCs has increased from 3.8% in 2009 to 22.7% in 2017.[5,6] Despite the high efficiency of PSCs, two challenges currently hinder their upscaling toward practical applications.[7] One issue is the long-term instability of PSCs, which is mainly caused by the intrinsic thermal instability of hybrid perovskite materials.[8−13] Encouragingly, it has been demonstrated recently that mixing the cations or replacing the organic cation with an inorganic cation can improve thermal stability and photostability (e.g., substituting FA for MA in $MAPbI_3$, Rb for Cs in $CsSnI_3$, and Cs for MA in $MAPbI_3$; MA stands for CH_3NH_3, and FA stands for NH_2CHNH_2).[7,14,15] The other concern is the well-documented toxicity of lead (Pb), which is particularly problematic because lead halide perovskites decompose into lead compounds that have significant solubility in water.[16] Consequently, an intensive research effort focused on finding air-stable lead-free perovskites suitable as the light-harvesting semiconductor in PSCs is now underway.[9,17−20]

Among the various alternatives to lead, tin (Sn) is regarded as a promising substitute because Sn-based hybrid perovskites have been shown to exhibit outstanding electrical and optical properties, including high charge carrier mobilities, high absorption coefficients, and low exciton binding energies.[21−23] Theoretical predictions by Even et al.[24] and Chiarella et al.[25] also confirmed the promising properties of Sn perovskites, such as suitable band gaps and favorable effective mass. However, Sn-based perovskites also have drawbacks, which have limited their application in efficient PSCs.[1,23,26−29] The primary challenge is the susceptibility of tin toward oxidation from the +2 to the +4 oxidation state upon exposure to ambient air, which, in the case of $CsSnI_3$, ultimately results in the formation of Cs_2SnI_6, whose relatively weak light absorption across the visible spectrum is undesirable for a photoabsorber.[22,30−33] Consequently, to date, there has been much less research effort directed at the advancement of tin halide PSCs than their lead analogues, and their PCE has remained below 10%.[27,28] Recently, a PCE as high as 9.0% in PSCs was achieved using single-crystalline $FASnI_3$, made by mixing a small amount of two-dimensional (2D) Sn perovskites with three-dimensional (3D) $FASnI_3$ in which the organic FA molecules are oriented randomly,[34] an approach that promises further improvement.

As compared to hybrid organic−inorganic Sn perovskites, all-inorganic Sn perovskites could have the advantage of

Received: April 27, 2018
Revised: June 29, 2018
Published: July 17, 2018

DOI: 10.1021/acs.jpcc.8b04013
J. Phys. Chem. C 2018, 122, 17660−17667

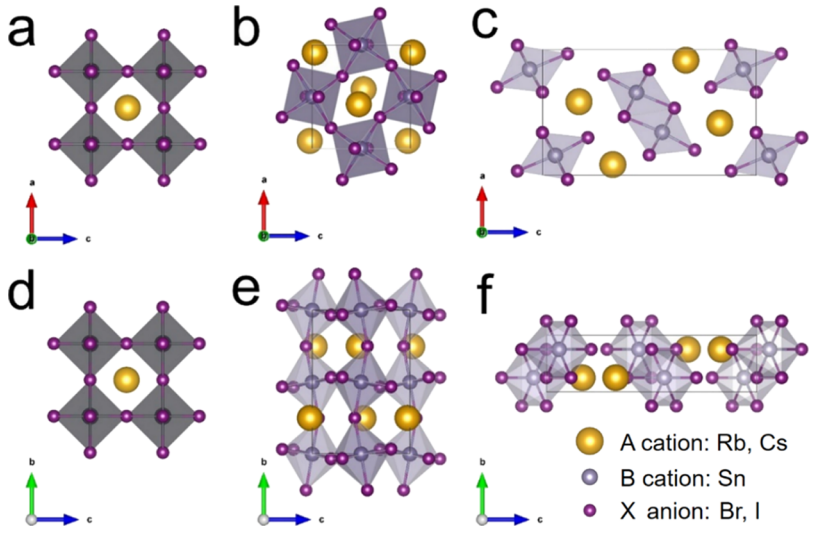

Figure 1. Top (a–c) and side (d–f) views of the cubic (α, *Pm*3*m*), orthorhombic (γ, *Pnma*), and yellow phase (Y, *Pnma*) of $ASnX_3$ (A = Cs and Rb and X = Br and I).

improved thermal stability while maintaining favorable optical and electronic properties for photovoltaic (PV) applications.[35,36] For example, γ-$CsSnI_3$ is a p-type semiconductor with a high hole mobility,[21,37] a favorable band gap of ~1.3 eV, a low exciton binding energy, and a high optical absorption coefficient.[38,39] There have been a few attempts to fabricate solar cells using γ-$CsSnI_3$ as a photoactive layer, but their maximum efficiency was still low. In 2012, Chen et al.[40] first used $CsSnI_3$ to fabricate a Schottky contact solar cell, which achieved a PCE of 0.9%. In 2014, Kumar et al.[41] achieved a PCE of 2.02% by forming the perovskite from a solution under Sn-rich conditions, using SnF_2 as the source of excess Sn, an approach that reduces the density of Sn vacancy defects. In 2016, Wang et al.[19] achieved a PCE of 3.31%. By removing the electron-blocking layer in a simplified inverted solar cell architecture and using the additive $SnCl_2$ instead of SnF_2, Marshall et al.[22] achieved the highest PCE to date of 3.56%, together with exceptional device stability under continuous illumination without device encapsulation. However, the PCE of γ-$CsSnI_3$-based solar cells is still significantly lower than those of their hybrid organic–inorganic Sn and Pb perovskite counterparts, primarily because of the lower open-circuit voltage. The most important challenges are therefore to develop ways to increase the open-circuit voltage and to stabilize tin halide perovskites toward oxidation in air. The oxidation instability manifests as a phase transition from the photoactive black orthorhombic (γ) phase to a photoinactive 2D yellow (Y) phase upon exposure to water vapor, which spontaneously converts to the weakly absorbing one-dimensional Cs_2SnI_6,[22] leading to difficulties in controlling the morphology and quality of the perovskite film.

In Pb halide perovskites, the strategy of mixing cations or anions has been widely used to improve the stability and PV performance of PSCs.[12,42–47] In contrast, explorations of the mixing of cations and anions in all-inorganic Sn-based perovskites are scarce.[7,48–50] Recently, the electronic structure variation of γ-$CsSnI_3$ by mixing A-site cations (e.g., mixing Cs and Rb) has been investigated by Jung et al.[7] However, the relative stability of the structures as compared to the Y phase was not investigated. To our knowledge, the amalgamated effect of exchange of both the A-site metal cation and the halide anion in completely inorganic tin perovskites has not been investigated.

In this paper, we present a theoretical study of the impact of cation and anion mixing (Rb/Cs cation exchange and Br/I anion exchange) in all-organic γ-$CsSnI_3$ using the density functional theory (DFT)-1/2 method [the local density approximation (LDA)-1/2 version],[51–54] taking into account the spin–orbit coupling (SOC) effect. We focus on the evolution of the electronic properties as well as the thermal and structural stabilities when substituting Br for I and Rb for Cs in γ-$CsSnI_3$. We predict that 3D perovskites with the composition $Rb_yCs_{1-y}Sn(Br_xI_{1-x})_3$, where $0 \le x,y \le 1$, are direct band gap semiconductors with band gaps in the range 1.3–2.0 eV. Importantly, our results indicate that substitution of Br for I in $CsSnI_3$ can prevent the unwanted γ-to-Y phase transition, evidenced by the favorable formation energies of the γ phase over the Y phase. In addition, calculations of the free energy of mixing and the prediction of phase diagram demonstrate that further substitution of Rb for Cs in $CsSn(Br_xI_{1-x})_3$ can improve the mixing thermodynamics, which is expected to improve the film-forming properties. Our predicted trends in the thermodynamic stability and band gaps provide a guideline to develop more efficient and stable lead-free all-inorganic perovskites for PSCs.

COMPUTATIONAL METHODS AND STRUCTURAL MODELS

The initial structure optimizations are performed using DFT as implemented in the Vienna ab initio simulation package (VASP).[55,56] The Perdew, Burke, and Ernzerhof (PBE) functional within the generalized gradient approximation is used.[57] The outermost s, p, and d (in the case of Sn) electrons are treated as valence electrons, whose interactions with the remaining ions are modeled by pseudopotentials generated within the projector-augmented wave method.[58,59] Figure 1 shows the crystal structures and cells used in the DFT calculations. Unit cells with 20 atoms (four $ASnX_3$ units) are used for all structures using a 1 × 1 × 1 cell for the γ and Y phases and 2 × 2 × 1 supercells for the α phase. In the structural optimization, the positions of the atoms as well as the cell volume and cell shape are all allowed to relax by setting

DOI: 10.1021/acs.jpcc.8b04013
J. Phys. Chem. C 2018, 122, 17660–17667

Table 1. Lattice Constants (in Å) Obtained by DFT and Band Gap Energies E_g (in eV) Obtained with the DFT-1/2 Method Including SOC Compared to Experimental Data and Theoretical Predictions Based on Hybrid and GW Methods

material	lattice constants (this work)	lattice constants (experimental)	lattice constants (other theoretical work)	E_g DFT-1/2 + SOC	E_g (experimental)	E_g + SOC
γ-$CsSnI_3$	8.99, 12.52, 8.63	8.69, 12.38, 8.64[a]	8.94, 12.52, 8.69[b]	1.36	1.27[c]	1.34 (GW_0)[d]
γ-$RbSnI_3$	8.91, 12.28, 8.47		8.93, 12.28, 8.47[b]	1.55		1.13 (HSE06)[b]
γ-$CsSnBr_3$	8.36, 11.79, 8.22			1.72		1.83 (GW_0)[d]
γ-$RbSnBr_3$	8.38, 11.55, 7.98			2.01		

[a]Reference 38. [b]Reference 7. [c]Reference 49. [d]Reference 68.

ISIF = 3. An energy cutoff of 500 eV and 4 × 4 × 8, 6 × 4 × 6, and 4 × 10 × 2 k-point meshes (α, γ, and Y phase structures, respectively) are used to achieve an energy and force convergence of 0.1 meV and 2 meV/Å, respectively. The subsequent electronic structure calculations were performed using an efficient approximate quasi-particle DFT method, namely, the DFT-1/2 method. The DFT-1/2 method stems from Slater's proposal of an approximation for the excitation energy, a transition-state method,[60,61] to reduce the band gap inaccuracy by introducing a half-electron/half-hole occupation. Teles et al.[51−54] extended the method to modern DFT and particularly to solid-state systems. Recently, we successfully applied this method in predicting accurate band gaps of metal halide perovskites.[62] The computational effort is the same as for standard DFT, with a straightforward inclusion of SOC when coupled with VASP. In this work, we extend the use of the DFT-1/2 method with the same settings (CUT values of 2.30, 3.34, and 3.76 for Sn, I, and Br, respectively, with half-ionized p orbitals) to alloys of $CsSnI_3$ when mixing Cs with Rb and I with Br. The physical insights of why Sn p and halide I or Br p orbitals are both half-ionized are demonstrated in Figure S1.

We calculated the free energy[7,63] of mixing for each composition according to the expression

$$\Delta F = \Delta U - T\Delta S \quad (1)$$

where ΔU and ΔS are the internal energy and entropy of mixing, respectively, and T is the absolute temperature. The internal energy of mixing of $Rb_xCs_{1-x}SnX_3$ is then calculated via the formula

$$\Delta U = E_{Rb_xCs_{1-x}SnX_3} - xE_{RbSnX_3} - (1-x)E_{CsSnX_3} \quad (2)$$

where $E_{Rb_xCs_{1-x}SnX_3}$, E_{RbSnX_3}, and E_{CsSnX_3} are the total energies of $Rb_xCs_{1-x}SnX_3$, $RbSnX_3$, and $CsSnX_3$, respectively.

The internal energy of mixing of $ASn(Br_xI_{1-x})_3$ is calculated using the formula

$$\Delta U = E_{ASn(Br_xI_{1-x})_3} - xE_{ASnBr_3} - (1-x)E_{ASnI_3} \quad (3)$$

where $E_{ASn(Br_xI_{1-x})_3}$, E_{ASnBr_3}, and E_{ASnI_3} are the total energies of $ASn(Br_xI_{1-x})_3$, $ASnBr_3$, and $ASnI_3$, respectively.

The entropy of mixing is calculated in the homogeneous limit according to the formula

$$\Delta S = -k_B[x \ln x + (1-x)\ln(1-x)] \quad (4)$$

where k_B is the Boltzmann constant.

We plot the phase diagram by using the generalized quasi-chemical approximation (GQCA)[63,64] code developed by Walsh et al.[63] to further investigate the thermodynamic properties of γ-$ASnX_3$. The phase diagram offers insight into the critical temperature for mixing and into the stability of the solid solution for typical temperatures at which perovskites are synthesized.

On the basis of the size of the cells for calculations, we have considered seven ($ASn(Br_xI_{1-x})_3$, x = 0, 1/6, 1/3, 1/2, 2/3, 5/6, and 1) and five ($Rb_yCs_{1-y}SnX_3$, y = 0, 1/4, 1/2, 3/4, and 1) concentrations of A cations and X anions, respectively. For the γ phase structures, all possible configurations (2, 4, and 2 for y = 1/4, 1/2, and 3/4, respectively) of substituting Rb for Cs were considered. Owing to the large number of possible configurations of substituting Br for I (22, 139, 252, 139, and 22 possible configurations for x = 1/6, 1/3, 1/2, 2/3, and 5/6, respectively), we have considered only two possible configurations for each concentration of Br, namely, the two extreme cases with most negative and least negative ΔH. From Figure S2 and Table S1, the formation energy of configuration 3 is the most negative, whereas that of configuration 7 is the least negative. This indicates that the Br ions tend to sit as close as possible to each other and to form as many bonds as possible with Sn ions. We use this strategy to select two extreme configurations for all other Br−I alloys considered in this work.

RESULTS AND DISCUSSION

Before studying the mixing of A cations and X anions in $ASnX_3$, we first performed calculations for the four pure compounds: $CsSnI_3$, $CsSnBr_3$, $RbSnI_3$, and $RbSnBr_3$. The calculated lattice parameters of orthorhombic (γ) $ASnX_3$ are shown in Table 1. Those of other polymorphs including cubic α, tetragonal β, and Y phase structures are listed in Table S2. The optimized lattice parameters are in good agreement with experiments, with a slight overestimation of lattice constants by about 1%, and with other theoretical results (differences within 0.1%).[7,38,49,65−68] It should be noted here that the predicted lattice parameters of α-$CsSnI_3$ and γ-$CsSnI_3$ in our previous work are smaller because of the use of LDA, which slightly underestimates the lattice parameters.[62] In this work, PBE is used, resulting in a slight overestimation of lattice parameters. Consequently, the predicted band gap of γ-$CsSnI_3$ (1.36 eV) in this work (will be discussed in the next paragraph) is slightly higher compared to that of previous work (1.34 eV).[62]

The calculated band gaps of γ-$CsSnI_3$ and γ-$CsSnBr_3$ are 1.36 and 1.72 eV, respectively, in excellent agreement with reported experimental measurements[49] (1.27 and 1.75 eV) and GW_0 calculations[68] (1.34 and 1.83 eV). There are no experimental reports known to us of the band gap of either $RbSnI_3$ or $RbSnBr_3$. Only theoretical results from HSE06 for γ-$RbSnI_3$ and PBE for α-$RbSnBr_3$ are found to be 1.41 and 0.57 eV, respectively.[7,69] Our predicted band gap for γ-$RbSnI_3$ is 1.55 eV. Substituting Br for I in γ-$RbSnI_3$ further increases the band gap to 2.01 eV.

It is worth noting that although $CsSnBr_3$ is reported to have the α structure at room temperature, the actual atomic arrangement at finite temperature (due to the dynamic

DOI: 10.1021/acs.jpcc.8b04013
J. Phys. Chem. C 2018, 122, 17660−17667

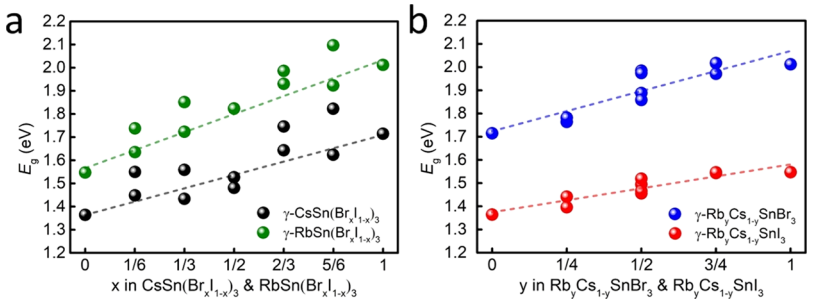

Figure 2. Calculated band gaps of (a) γ-ASn(Br$_x$I$_{1-x}$)$_3$ and (b) γ-Rb$_y$Cs$_{1-y}$SnX$_3$ perovskites. The dashed lines are guides to the eye.

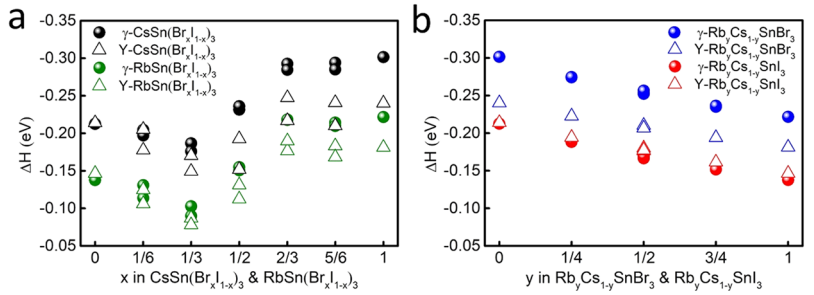

Figure 3. Formation energy (ΔH) of (a) ASn(Br$_x$I$_{1-x}$)$_3$ and (b) Rb$_y$Cs$_{1-y}$SnX$_3$ perovskites for the γ and Y phases. Because of the large number of possible configurations for each substitution concentration x of Br in ASn(Br$_x$I$_{1-x}$)$_3$, we only show in (a) the results for the two configurations with the most negative and least negative ΔH.

disorder of the ions in the lattice)[70] resembles that of the γ phase. Consequently, it is not surprising that predicted band gaps using α structures are always significantly smaller than those measured experimentally.[7,24,71,72] Therefore, in this work, we always report band gaps calculated using γ phases. RbSnI$_3$ has been reported to exist in a nonperovskite 2D Y phase structure owing to the small cationic size of Rb$^+$.[38,66] Nevertheless, for comparison with the alloys Rb$_y$Cs$_{1-y}$SnI$_3$, the band gaps of RbSnI$_3$ in a 3D γ phase are also predicted. In addition, all band gaps of α structures are also provided in the Supporting Information in Table S2 and Figure S3 for comparison. The calculated effective masses of the electrons and holes at the G point for γ-ASnX$_3$ are given in Table S3.

Figure 2 shows the computed band gaps for the γ phases of ASn(Br$_x$I$_{1-x}$)$_3$ and Rb$_y$Cs$_{1-y}$SnX$_3$ perovskites, whereas the band gaps of the other structures are shown in Figure S4. In general, the band gap increases with increasing percentage of Br in ASn(Br$_x$I$_{1-x}$)$_3$ and Rb in Rb$_y$Cs$_{1-y}$SnX$_3$. From Figure 2a and Table S4, generally, the band gaps change because of the variations in both volume and lattice distortion. However, the changes in cell volume have more pronounced effects on the band gaps than the changes in lattice distortion, that is, octahedral tilting. The reduction of the cell volume is responsible for the widening of the band gap in ASn(Br$_x$I$_{1-x}$)$_3$ or Rb$_y$Cs$_{1-y}$SnX$_3$ solid solutions with an increased Br or Rb percentage. For the band gap variations with the same Br or Rb percentage in ASn(Br$_x$I$_{1-x}$)$_3$ or Rb$_y$Cs$_{1-y}$SnX$_3$ solid solutions, there is no certain relationship found between the degree of lattice distortion (i.e., the degree of octahedral tilting, which is the tilting angle difference $|\Delta\bar{\theta}|$)[4] and band gaps.

It is well-known that for single-junction and multijunction solar cells, the Shockley–Queisser limit suggests optimal band gap ranges of 0.9–1.6 and 1.6–2.0 eV, respectively, for achieving a maximum PCE.[23,73] The band gaps of CsSn(Br$_x$I$_{1-x}$)$_3$ are almost completely in the optimal range (1.30–1.55 eV) for single-junction PSCs. When substituting Rb for Cs in CsSn(Br$_x$I$_{1-x}$)$_3$, the band gaps of RbSn(Br$_x$I$_{1-x}$)$_3$ increase by 0.2–0.3 eV as compared to their Cs counterparts, making RbSn(Br$_x$I$_{1-x}$)$_3$ ($x > 1/3$) ideal as a wide-band gap material for tandem solar cells in conjunction with narrow-band gap semiconductors such as Si or CsSn(Br$_x$I$_{1-x}$)$_3$. The changes in band gap when mixing Rb and Cs cations are much smaller than those when mixing I and Br. This is true for all values $0 \leq y \leq 1$ and also for different structures with a fixed y. The band gaps of Rb$_y$Cs$_{1-y}$SnBr$_3$ (1.71–2.01 eV) and Rb$_y$Cs$_{1-y}$SnI$_3$ (1.36–1.55 eV) are in the ideal range for tandem and single-junction solar cells, respectively.

In addition to the band gap, another key property for the application of mixed inorganic perovskites in PSCs is their structural stability. CsSnI$_3$ has two coexisting polymorphs (the γ and Y phases) at room temperature, which both belong to the *Pnma* space group. Although both phases have similar free energies and stable phonon modes, a transition from the black γ phase to the yellow Y phase has been observed in ambient conditions.[7,38,74] Oxidation of Sn^{2+} to Sn^{4+} spontaneously occurs after the transformation of the γ phase to the Y phase.[75]

Because of the different crystal structure and electronic properties of the Y phase (i.e., a 2D structure and an indirect band gap of 2.6 eV), the unwanted phase transition from γ to Y can considerably decrease the efficiency of a solar cell.[14,22,75–77] In addition, the Y phase will spontaneously react with O$_2$ when exposed to air, resulting in Cs$_2$SnI$_6$ with a face-centered cubic structure.[30,32] Therefore, we focus here on the evolution of the stability of the γ and Y phases upon gradual substitution of Br for I and Rb for Cs. The results of our calculations for other structures are given in Figure S5.

The formation energy of ASnX$_3$ is defined as $\Delta H = E_{ASnX_3} - E_{AX} - E_{SnX_2}$, where E_{ASnX_3}, E_{AX}, and E_{SnX_2} are the total energies of ASnX$_3$, AX, and SnX$_2$, respectively. Here, a negative value of ΔH represents favorable formation of ASnX$_3$ perovskites. The

DOI: 10.1021/acs.jpcc.8b04013
J. Phys. Chem. C 2018, 122, 17660–17667

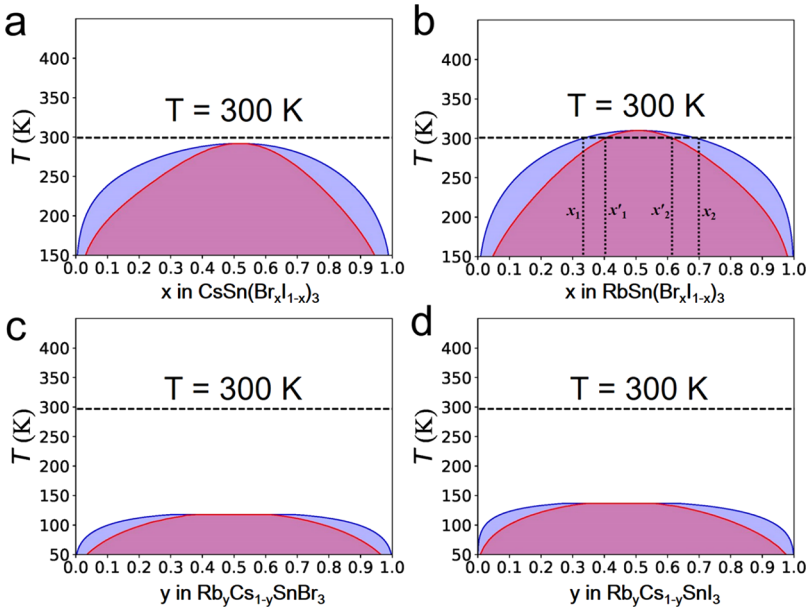

Figure 4. Predicted phase diagrams of (a) γ-CsSn(Br$_x$I$_{1-x}$)$_3$, (b) γ-RbSn(Br$_x$I$_{1-x}$)$_3$, (c) γ-Rb$_y$Cs$_{1-y}$SnBr$_3$, and (d) γ-Rb$_y$Cs$_{1-y}$SnI$_3$ solid solutions. The purple and pink lines are binodals and spinodals, respectively. The dashed horizontal lines indicate room temperature (300 K). In (b), the gap between the horizontal line and the critical miscibility temperature is the miscibility gap in γ-RbSn(Br$_x$I$_{1-x}$)$_3$. A thermodynamically stable solid solution can be formed only in the white region.

more negative ΔH, the more stable the corresponding structure. It can be clearly seen in Figure 3 that all perovskites considered exhibit good thermal stability, with large negative ΔH values. Figure 3 also shows the effect of ion mixing on the stability of the γ phase with respect to the Y phase.

For CsSnI$_3$, the formation energies of the γ and Y phases are the same. However, with the increase of Rb concentration, the structural instability of Rb$_y$Cs$_{1-y}$SnI$_3$ becomes increasingly pronounced. Consequently, upon exposure to air, the rate at which the perovskite oxidizes is predicated to increase with an increasing Rb concentration.[75] The substitution of Rb for Cs seems to facilitate the formation of the Y phase, as now evidenced by the more negative formation energy of the Y phase than the γ phase. It should be mentioned that the formation energies are both negative for RbSnI$_3$ in both γ and Y phases. However, the formation energy of the Y phase is relatively more negative, indicating that the Y phase is more favorable than the γ phase. Indeed, the instability of the γ phase is in agreement with the experimental observation of RbSnI$_3$ only existing in a 2D yellow phase.[75] On the contrary, for CsSnBr$_3$, the formation energy of the Y phase is much less negative than that of the γ phase (by 0.06 eV), indicating that the γ phase is more stable than the Y phase. The substitution of Rb for Cs results in a slight decrease (to 0.04 eV) in the energy differences between the two phases, with the γ phase still being favored.

The formation energies of mixing Cs and Rb in Rb$_y$Cs$_{1-y}$SnI$_3$ or Rb$_y$Cs$_{1-y}$SnBr$_3$ follow a perfect linear relation (Figure 3b), indicating favorable mixing thermodynamics. However, substitution of Br for I (Figure 3a) shows an unusual trend as a function of x: the curves show first a decrease and then an increase, with a valley point at $x = 1/3$ in both CsSn(Br$_x$I$_{1-x}$)$_3$ and RbSn(Br$_x$I$_{1-x}$)$_3$. When $x < 1/3$, the most negative ΔH of the γ phase for each concentration is relatively more positive than or nearly equal to the most negative ΔH of the Y phase, which indicates that the Y phase is favored over the γ phase. When $x = 1/3$, the most negative ΔH of the γ phase is clearly more negative than the most negative ΔH of the Y phase, whereas the least negative ΔH of the γ phase is almost equal to the most negative ΔH of the Y phase. When $x > 1/3$, all ΔH of the γ phase for each concentration are more negative than those of the Y phase, which means that the γ phase is stabilized. For Rb$_y$Cs$_{1-y}$SnI$_3$ or Rb$_y$Cs$_{1-y}$SnBr$_3$, mixing Cs and Rb does not change the stability of the γ phase with respect to the Y phase (Figure 3b). For Rb$_y$Cs$_{1-y}$SnI$_3$, the Y phase is always favored when mixing Rb and Cs, whereas for Rb$_y$Cs$_{1-y}$SnBr$_3$, the opposite is true. We conclude that the addition of Br to Rb$_y$Cs$_{1-y}$SnI$_3$ tends to stabilize the favorable γ phase and suppress the transformation to the Y phase. The critical Br concentration is about one-third. This prediction calls for an experimental validation.

As shown in Figure 3, very different trends are observed for mixing of cations (Rb and Cs) and anions (I and Br) in γ-CsSnI$_3$. For a deeper insight, we have investigated the different mixing thermodynamics by calculating the Helmholtz free energy of mixing. Details of the calculations can be found in the Computational Methods and Structural Models section. Results of these calculations are shown in Figure S6. On the basis of the Helmholtz free energies, we plot the phase diagram for γ-ASnX$_3$ by using the GQCA[63] code, as shown in Figure 4.

For CsSn(Br$_x$I$_{1-x}$)$_3$, the critical temperature is 291 K (see Figure 4a), indicating that the mixing of anions (I and Br) is favorable at room temperature (300 K). However, for RbSn(Br$_x$I$_{1-x}$)$_3$ at 300 K, a miscibility gap is found in the composition region between $x_1 = 0.33$ and $x_2 = 0.70$ (see Figure 4b). The pure compounds RbSnI$_3$ and RbSnBr$_3$ are not miscible inside the miscibility gap under equilibrium conditions, leading to the formation of two phases with Br concentrations x_1 and x_2. Meanwhile, the alloy has spinodal points at the compositions $x'_1 = 0.40$ and $x'_2 = 0.62$ at room temperature. Thus, in the intervals $x_1 < x < x'_1$ and $x'_2 < x < x_2$, a metastable phase can occur, showing small fluctuations in composition. The predicted critical temperature (the temperature above which the solid solution is stable for any

DOI: 10.1021/acs.jpcc.8b04013
J. Phys. Chem. C 2018, 122, 17660−17667

composition) is 312 K, which is significantly lower than the critical temperature of 343 K predicted for the $MAPb(Br_xI_{1-x})_3$ perovskite.[63] This indicates that, although mixing of Br and I is not favored slightly below (for $CsSn(Br_xI_{1-x})_3$) or around (for $RbSn(Br_xI_{1-x})_3$) room temperature, the phase segregation in these alloys is less significant than that in $MAPb(Br_xI_{1-x})_3$ perovskites.

A uniform mixture can be synthesized either through control of the deposition kinetics or by annealing above the critical miscibility temperature. The uniform mixture tends to segregate below the critical temperature, but this segregation is a very slow process.[63] The inclusion of smaller cations often provides an improvement, overcoming kinetic barriers and changing the local critical temperature. For example, smaller cations such as Cs and Rb were introduced in (FA/MA)Pb(I/Br)$_3$ and were shown to have a positive effect on the structural and photostability of state-of-the-art PSCs.[8,10,13,78] Indeed, we predict that mixing of Rb and Cs in $Rb_yCs_{1-y}SnX_3$ is very favorable at room temperature. For $Rb_yCs_{1-y}SnBr_3$ and $Rb_yCs_{1-y}SnI_3$, the phase diagrams show that mixing of cations (Rb and Cs) is favorable at temperatures above 118 and 137 K, respectively (see Figure 4c,d). Our prediction of the critical miscibility temperature of 137 K of $Rb_yCs_{1-y}SnI_3$ is in good agreement with the result of 140 K calculated by Jung et al.[7] The slight difference of the predicted critical temperature could be caused by the small variation in energies per cell due to the differences in computational settings (energy cutoff value, k-point grid, version, and implementation of VASP codes) in DFT calculations. The critical temperatures of mixing of Rb and Cs in $Rb_yCs_{1-y}SnX_3$ are much lower than those of mixing of Br and I in $ASn(Br_xI_{1-x})_3$. Therefore, additional mixing of Cs and Rb in $ASnI_xBr_{1-x}$ is predicted to bring down the critical temperature for mixing of Br and I below room temperature, suppressing phase segregation and resulting in better material quality for PV applications.

CONCLUSIONS

In summary, the effects of cation (Cs and Rb) and anion (I and Br) mixing in all-inorganic tin halide perovskites have been investigated with DFT-based calculations. Using standard DFT for structure optimization and the DFT-1/2 method with SOC for band structure calculations, we studied the evolution of the structural, thermodynamic, and electronic properties as a function of the extent of substitution of Rb for Cs and Br for I. We predict that $Cs_yRb_{1-y}Sn(Br_xI_{1-x})_3$ perovskites have direct band gaps in the range of 1.3−2.0 eV. The alloys with high I and Cs concentrations are well suited for highly efficient single-junction PSCs, whereas those with high Rb and Br concentrations are suitable as wide-band gap materials for tandem PSCs. Importantly, we found that substitution of Br for I can suppress the unwanted γ-to-Y phase transition. The critical concentration for stabilization of the γ phase with respect to the Y phase in $Cs_yRb_{1-y}Sn(Br_xI_{1-x})_3$ is $x = 1/3$. Furthermore, phase diagrams based on the free energy of mixing show that a solid solution of Br and I is thermodynamically possible around and slightly above room temperature for $CsSn(Br_xI_{1-x})_3$ and $RbSn(Br_xI_{1-x})_3$, respectively. Finally, substitution of Rb for Cs to $ASn(Br_xI_{1-x})_3$ is predicted to decrease the critical temperature to well below room temperature, enabling the formation of highly homogeneous solid solutions for improved solar cell performance. Our predictions regarding the stabilization of the γ phase and the use of five elements in $Rb_yCs_{1-y}Sn(Br_xI_{1-x})_3$ as an efficient and stable light absorber for PSCs call for experimental exploration.

ASSOCIATED CONTENT

Supporting Information

The Supporting Information is available free of charge on the ACS Publications website at DOI: 10.1021/acs.jpcc.8b04013.

Physical insights of why Sn p and halide I or Br p orbitals are both half-ionized; illustration of the selection strategy of $ASn(Br_xI_{1-x})_3$ to reduce computational effort; summary of lattice constants and band gaps (E_g) of polymorphs of $ASnX_3$ ($CsSnI_3$, $RbSnI_3$, $CsSnBr_3$, and $RbSnBr_3$); band structures for $CsSnI_3$, $CsSnBr_3$, $RbSnI_3$, and $RbSnBr_3$ with the γ phase and the α phase; effective masses for γ-$CsSnI_3$, γ-$CsSnBr_3$, γ-$RbSnI_3$, and γ-$RbSnBr_3$; average tilting angles and cell volumes of γ-$CsSn(Br_xI_{1-x})_3$, γ-$RbSn(Br_xI_{1-x})_3$, γ-$Rb_yCs_{1-y}SnBr_3$, and γ-$Rb_yCs_{1-y}SnI_3$; band gaps and formation energies of $ASn(Br_xI_{1-x})_3$ and $Rb_yCs_{1-y}SnX_3$ perovskites, including the α phase; and Helmholtz free energy of mixing of α and γ polymorphs (PDF)

AUTHOR INFORMATION

Corresponding Author

*E-mail: s.x.tao@tue.nl.

ORCID

Junke Jiang: 0000-0003-2962-766X

Ross A. Hatton: 0000-0002-8851-1280

Shuxia Tao: 0000-0002-3658-8497

Notes

The authors declare no competing financial interest.

ACKNOWLEDGMENTS

S.T. and J.J. acknowledge the funding by the Computational Sciences for Energy Research (CSER) tenure track program of Shell, NWO, and FOM (Project number 15CST04-2). Dr. Peter Klaver is acknowledged for his technical support in the computational study in this work.

REFERENCES

(1) Yablonovitch, E. Lead Halides Join the Top Optoelectronic League. *Science* **2016**, *351*, 1401.

(2) Green, M. A.; Ho-Baillie, A.; Snaith, H. J. The Emergence of Perovskite Solar Cells. *Nat. Photonics* **2014**, *8*, 506−514.

(3) Kadro, J. M.; Pellet, N.; Giordano, F.; Ulianov, A.; Müntener, O.; Maier, J.; Grätzel, M.; Hagfeldt, A. Proof-of-Concept for Facile Perovskite Solar Cell Recycling. *Energy Environ. Sci.* **2016**, *9*, 3172−3179.

(4) Pedesseau, L.; Sapori, D.; Traore, B.; Robles, R.; Fang, H.-H.; Loi, M. A.; Tsai, H.; Nie, W.; Blancon, J.-C.; Neukirch, A.; et al. Advances and Promises of Layered Halide Hybrid Perovskite Semiconductors. *ACS Nano* **2016**, *10*, 9776−9786.

(5) Kojima, A.; Teshima, K.; Shirai, Y.; Miyasaka, T. Organometal Halide Perovskites as Visible-Light Sensitizers for Photovoltaic Cells. *J. Am. Chem. Soc.* **2009**, *131*, 6050−6051.

(6) National Renewable Energy Laboratory. Best Research-Cell Efficiencies. https://www.nrel.gov/pv/assets/images/efficiency-chart.png (accessed March 21, 2018).

(7) Jung, Y.-K.; Lee, J.-H.; Walsh, A.; Soon, A. Influence of Rb/Cs Cation-Exchange on Inorganic Sn Halide Perovskites: From Chemical Structure to Physical Properties. *Chem. Mater.* **2017**, *29*, 3181−3188.

DOI: 10.1021/acs.jpcc.8b04013
J. Phys. Chem. C 2018, 122, 17660−17667

(8) Liang, L.; Gao, P. Lead-Free Hybrid Perovskite Absorbers for Viable Application: Can We Eat the Cake and Have It too? *Adv. Sci.* **2017**, *5*, 1700331.
(9) Wang, A.; Guo, Y.; Muhammad, F.; Deng, Z. Controlled Synthesis of Lead-Free Cesium Tin Halide Perovskite Cubic Nanocages with High Stability. *Chem. Mater.* **2017**, *29*, 6493−6501.
(10) Whalley, L. D.; Frost, J. M.; Jung, Y.-K.; Walsh, A. Perspective: Theory and Simulation of Hybrid Halide Perovskites. *J. Chem. Phys.* **2017**, *146*, 220901.
(11) Sun, Q.; Yin, W.-J. Thermodynamic Stability Trend of Cubic Perovskites. *J. Am. Chem. Soc.* **2017**, *139*, 14905−14908.
(12) Gratia, P.; Grancini, G.; Audinot, J.-N.; Jeanbourquin, X.; Mosconi, E.; Zimmermann, I.; Dowsett, D.; Lee, Y.; Grätzel, M.; De Angelis, F.; et al. Intrinsic Halide Segregation at Nanometer Scale Determines the High Efficiency of Mixed Cation/Mixed Halide Perovskite Solar Cells. *J. Am. Chem. Soc.* **2016**, *138*, 15821−15824.
(13) Correa-Baena, J.-P.; Abate, A.; Saliba, M.; Tress, W.; Jesper Jacobsson, T.; Grätzel, M.; Hagfeldt, A. The Rapid Evolution of Highly Efficient Perovskite Solar Cells. *Energy Environ. Sci.* **2017**, *10*, 710−727.
(14) Yi, C.; Luo, J.; Meloni, S.; Boziki, A.; Ashari-Astani, N.; Grätzel, C.; Zakeeruddin, S. M.; Röthlisberger, U.; Grätzel, M. Entropic stabilization of mixed A-cation ABX_3 metal halide perovskites for high performance perovskite solar cells. *Energy Environ. Sci.* **2016**, *9*, 656−662.
(15) Niemann, R. G.; Gouda, L.; Hu, J.; Tirosh, S.; Gottesman, R.; Cameron, P. J.; Zaban, A. Cs+ incorporation into $CH_3NH_3PbI_3$ perovskite: substitution limit and stability enhancement. *J. Mater. Chem. A* **2016**, *4*, 17819−17827.
(16) Babayigit, A.; Ethirajan, A.; Muller, M.; Conings, B. Toxicity of Organometal Halide Perovskite Solar Cells. *Nat. Mater.* **2016**, *15*, 247−251.
(17) Ju, M.-G.; Chen, M.; Zhou, Y.; Garces, H. F.; Dai, J.; Ma, L.; Padture, N. P.; Zeng, X. C. Earth-Abundant Nontoxic Titanium(IV)-based Vacancy-Ordered Double Perovskite Halides with Tunable 1.0 to 1.8 eV Bandgaps for Photovoltaic Applications. *ACS Energy Lett.* **2018**, *3*, 297−304.
(18) Shi, Z.; Guo, J.; Chen, Y.; Li, Q.; Pan, Y.; Zhang, H.; Xia, Y.; Huang, W. Lead-Free Organic-Inorganic Hybrid Perovskites for Photovoltaic Applications: Recent Advances and Perspectives. *Adv. Mater.* **2017**, *29*, 1605005.
(19) Wang, N.; Zhou, Y.; Ju, M.-G.; Garces, H. F.; Ding, T.; Pang, S.; Zeng, X. C.; Padture, N. P.; Sun, X. W. Heterojunction-Depleted Lead-Free Perovskite Solar Cells with Coarse-Grained B-γ-$CsSnI_3$ Thin Films. *Adv. Energy Mater.* **2016**, *6*, 1601130.
(20) Harikesh, P. C.; Mulmudi, H. K.; Ghosh, B.; Goh, T. W.; Teng, Y. T.; Thirumal, K.; Lockrey, M.; Weber, K.; Koh, T. M.; Li, S.; et al. Rb as an Alternative Cation for Templating Inorganic Lead-Free Perovskites for Solution Processed Photovoltaics. *Chem. Mater.* **2016**, *28*, 7496−7504.
(21) Chung, I.; Lee, B.; He, J.; Chang, R. P. H.; Kanatzidis, M. G. All-Solid-State Dye-Sensitized Solar Cells with High Efficiency. *Nature* **2012**, *485*, 486−489.
(22) Marshall, K. P.; Walker, M.; Walton, R. I.; Hatton, R. A. Enhanced Stability and Efficiency in Hole-Transport-Layer-Free $CsSnI_3$ Perovskite Photovoltaics. *Nat. Energy* **2016**, *1*, 16178.
(23) Konstantakou, M.; Stergiopoulos, T. A Critical Review on Tin Halide Perovskite Solar Cells. *J. Mater. Chem. A* **2017**, *5*, 11518−11549.
(24) Even, J.; Pedesseau, L.; Jancu, J.-M.; Katan, C. DFT and modelling of the phase transitions of lead and tin halide perovskites for photovoltaic cells. *Phys. Status Solidi RRL* **2014**, *8*, 31−35.
(25) Chiarella, F.; Zappettini, A.; Licci, F.; Borriello, I.; Cantele, G.; Ninno, D.; Cassinese, A.; Vaglio, R. Combined Experimental and Theoretical Investigation of Optical, Structural, and Electronic Properties of $CH_3NH_3SnX_3$ Thin Films (X= Cl, Br). *Phys. Rev. B: Condens. Matter Mater. Phys.* **2008**, *77*, 045129.
(26) Abate, A. Perovskite Solar Cells Go Lead Free. *Joule* **2017**, *1*, 659−664.
(27) Noel, N. K.; Stranks, S. D.; Abate, A.; Wehrenfennig, C.; Guarnera, S.; Haghighirad, A.-A.; Sadhanala, A.; Eperon, G. E.; Pathak, S. K.; Johnston, M. B.; Petrozza, A.; Herz, L. M.; Snaith, H. J. Lead-free organic-inorganic tin halide perovskites for photovoltaic applications. *Energy Environ. Sci.* **2014**, *7*, 3061−3068.
(28) Hao, F.; Stoumpos, C. C.; Cao, D. H.; Chang, R. P. H.; Kanatzidis, M. G. Lead-Free Solid-State Organic-Inorganic Halide Perovskite Solar Cells. *Nat. Photonics* **2014**, *8*, 489−494.
(29) Sun, Y.-Y.; Shi, J.; Lian, J.; Gao, W.; Agiorgousis, M. L.; Zhang, P.; Zhang, S. Discovering Lead-free Perovskite Solar Materials with a Split-Anion Approach. *Nanoscale* **2016**, *8*, 6284−6289.
(30) Lee, B.; Stoumpos, C. C.; Zhou, N.; Hao, F.; Malliakas, C.; Yeh, C.-Y.; Marks, T. J.; Kanatzidis, M. G.; Chang, R. P. H. Air-Stable Molecular Semiconducting Iodosalts for Solar Cell Applications: Cs_2SnI_6 as a Hole Conductor. *J. Am. Chem. Soc.* **2014**, *136*, 15379−15385.
(31) Xiao, Z.; Zhou, Y.; Hosono, H.; Kamiya, T. Intrinsic defects in a photovoltaic perovskite variant Cs2SnI6. *Phys. Chem. Chem. Phys.* **2015**, *17*, 18900−18903.
(32) Saparov, B.; Sun, J.-P.; Meng, W.; Xiao, Z.; Duan, H.-S.; Gunawan, O.; Shin, D.; Hill, I. G.; Yan, Y.; Mitzi, D. B. Thin-Film Deposition and Characterization of a Sn-Deficient Perovskite Derivative Cs_2SnI_6. *Chem. Mater.* **2016**, *28*, 2315−2322.
(33) Qiu, X.; Cao, B.; Yuan, S.; Chen, X.; Qiu, Z.; Jiang, Y.; Ye, Q.; Wang, H.; Zeng, H.; Liu, J.; et al. From unstable $CsSnI_3$ to air-stable Cs_2SnI_6: A lead-free perovskite solar cell light absorber with bandgap of 1.48 eV and high absorption coefficient. *Sol. Energy Mater. Sol. Cells* **2017**, *159*, 227−234.
(34) Shao, S.; Liu, J.; Portale, G.; Fang, H.-H.; Blake, G. R.; ten Brink, G. H.; Koster, L. J. A.; Loi, M. A. Highly Reproducible Sn-Based Hybrid Perovskite Solar Cells with 9% Efficiency. *Adv. Energy Mater.* **2017**, *8*, 1702019.
(35) Gupta, S.; Bendikov, T.; Hodes, G.; Cahen, D. $CsSnBr_3$, A Lead-Free Halide Perovskite for Long-Term Solar Cell Application: Insights on SnF_2 Addition. *ACS Energy Lett.* **2016**, *1*, 1028−1033.
(36) Kontos, A. G.; Kaltzoglou, A.; Siranidi, E.; Palles, D.; Angeli, G. K.; Arfanis, M. K.; Psycharis, V.; Raptis, Y. S.; Kamitsos, E. I.; Trikalitis, P. N.; et al. Structural Stability, Vibrational Properties, and Photoluminescence in $CsSnI_3$ Perovskite upon the Addition of SnF_2. *Inorg. Chem.* **2017**, *56*, 84−91.
(37) Xu, P.; Chen, S.; Xiang, H.-J.; Gong, X.-G.; Wei, S.-H. Influence of Defects and Synthesis Conditions on the Photovoltaic Performance of Perovskite Semiconductor $CsSnI_3$. *Chem. Mater.* **2014**, *26*, 6068−6072.
(38) Chung, I.; Song, J.-H.; Im, J.; Androulakis, J.; Malliakas, C. D.; Li, H.; Freeman, A. J.; Kenney, J. T.; Kanatzidis, M. G. CsSnI3: Semiconductor or Metal? High Electrical Conductivity and Strong Near-Infrared Photoluminescence from a Single Material. High Hole Mobility and Phase-Transitions. *J. Am. Chem. Soc.* **2012**, *134*, 8579−8587.
(39) Huang, L.-y.; Lambrecht, W. R. L. Electronic Band Structure, Phonons, and Exciton Binding Energies of Halide Perovskites $CsSnCl_3$, $CsSnBr_3$, and $CsSnI_3$. *Phys. Rev. B: Condens. Matter Mater. Phys.* **2013**, *88*, 165203.
(40) Chen, Z.; Wang, J. J.; Ren, Y.; Yu, C.; Shum, K. Schottky solar cells based on $CsSnI_3$ thin-films. *Appl. Phys. Lett.* **2012**, *101*, 093901.
(41) Kumar, M. H.; Dharani, S.; Leong, W. L.; Boix, P. P.; Prabhakar, R. R.; Baikie, T.; Shi, C.; Ding, H.; Ramesh, R.; Asta, M.; Graetzel, M.; Mhaisalkar, S. G.; Mathews, N. Lead-Free Halide Perovskite Solar Cells with High Photocurrents Realized Through Vacancy Modulation. *Adv. Mater.* **2014**, *26*, 7122−7127.
(42) Ono, L. K.; Juarez-Perez, E. J.; Qi, Y. Progress on Perovskite Materials and Solar Cells with Mixed Cations and Halide Anions. *ACS Appl. Mater. Interfaces* **2017**, *9*, 30197−30246.
(43) Wang, Z.; McMeekin, D. P.; Sakai, N.; van Reenen, S.; Wojciechowski, K.; Patel, J. B.; Johnston, M. B.; Snaith, H. J. Efficient and Air-Stable Mixed-Cation Lead Mixed-Halide Perovskite Solar Cells with n-Doped Organic Electron Extraction Layers. *Adv. Mater.* **2017**, *29*, 1604186.

DOI: 10.1021/acs.jpcc.8b04013
J. Phys. Chem. C 2018, 122, 17660−17667

(44) Bi, D.; Tress, W.; Dar, M. I.; Gao, P.; Luo, J.; Renevier, C.; Schenk, K.; Abate, A.; Giordano, F.; Correa Baena, J.-P.; Decoppet, J.-D.; Zakeeruddin, S. M.; Nazeeruddin, M. K.; Grätzel, M.; Hagfeldt, A. Efficient Luminescent Solar Cells Based on Tailored Mixed-Cation Perovskites. *Sci. Adv.* **2016**, *2*, No. e1501170.
(45) Pellet, N.; Gao, P.; Gregori, G.; Yang, T.-Y.; Nazeeruddin, M. K.; Maier, J.; Grätzel, M. Mixed-Organic-Cation Perovskite Photovoltaics for Enhanced Solar-Light Harvesting. *Angew. Chem., Int. Ed.* **2014**, *53*, 3151−3157.
(46) Akkerman, Q. A.; D'Innocenzo, V.; Accornero, S.; Scarpellini, A.; Petrozza, A.; Prato, M.; Manna, L. Tuning the Optical Properties of Cesium Lead Halide Perovskite Nanocrystals by Anion Exchange Reactions. *J. Am. Chem. Soc.* **2015**, *137*, 10276−10281.
(47) McMeekin, D. P.; Sadoughi, G.; Rehman, W.; Eperon, G. E.; Saliba, M.; Horantner, M. T.; Haghighirad, A.; Sakai, N.; Korte, L.; Rech, B.; Johnston, M. B.; Herz, L. M.; Snaith, H. J. A Mixed-Cation Lead Mixed-Halide Perovskite Absorber for Tandem Solar Cells. *Science* **2016**, *351*, 151−155.
(48) Li, W.; Li, J.; Li, J.; Fan, J.; Mai, Y.; Wang, L. Addictive-assisted construction of all-inorganic $CsSnIBr_2$ mesoscopic perovskite solar cells with superior thermal stability up to 473 K. *J. Mater. Chem. A* **2016**, *4*, 17104−17110.
(49) Sabba, D.; Mulmudi, H. K.; Prabhakar, R. R.; Krishnamoorthy, T.; Baikie, T.; Boix, P. P.; Mhaisalkar, S.; Mathews, N. Impact of Anionic Br- Substitution on Open Circuit Voltage in Lead Free Perovskite ($CsSnI_{3-x}Br_x$) Solar Cells. *J. Phys. Chem. C* **2015**, *119*, 1763−1767.
(50) Saliba, M.; Matsui, T.; Domanski, K.; Seo, J.-Y.; Ummadisingu, A.; Zakeeruddin, S. M.; Correa-Baena, J.-P.; Tress, W. R.; Abate, A.; Hagfeldt, A.; Gratzel, M. Incorporation of Rubidium Cations into Perovskite Solar Cells Improves Photovoltaic Performance. *Science* **2016**, *354*, 206−209.
(51) Ferreira, L. G.; Marques, M.; Teles, L. K. Approximation to Density Functional Theory for the Calculation of Band Gaps of Semiconductors. *Phys. Rev. B: Condens. Matter Mater. Phys.* **2008**, *78*, 125116.
(52) Pelá, R. R.; Caetano, C.; Marques, M.; Ferreira, L. G.; Furthmüller, J.; Teles, L. K. Accurate Band Gaps of AlGaN, InGaN, and AlInN Alloys Calculations Based on LDA-1/2 Approach. *Appl. Phys. Lett.* **2011**, *98*, 151907.
(53) Ferreira, L. G.; Marques, M.; Teles, L. K. Slater Half-Occupation Technique Revisited: the LDA-1/2 and GGA-1/2 Approaches for Atomic Ionization Energies and Band Gaps in Semiconductors. *AIP Adv.* **2011**, *1*, 032119.
(54) Pela, R. R.; Marques, M.; Teles, L. K. Comparing LDA-1/2, HSE03, HSE06 and G_0W_0 approaches for band gap calculations of alloys. *J. Phys.: Condens. Matter* **2015**, *27*, 505502.
(55) Kresse, G.; Furthmüller, J. Efficiency of Ab-Initio Total Energy Calculations for Metals and Semiconductors Using a Plane-Wave Basis Set. *Comput. Mater. Sci.* **1996**, *6*, 15−50.
(56) Kresse, G.; Furthmüller, J. Efficient iterative schemes for ab initio total-energy calculations using a plane-wave basis set. *Phys. Rev. B: Condens. Matter Mater. Phys.* **1996**, *54*, 11169−11186.
(57) Perdew, J. P.; Burke, K.; Ernzerhof, M. Generalized Gradient Approximation Made Simple. *Phys. Rev. Lett.* **1996**, *77*, 3865−3868.
(58) Blöchl, P. E. Projector Augmented-Wave Method. *Phys. Rev. B: Condens. Matter Mater. Phys.* **1994**, *50*, 17953−17979.
(59) Kresse, G.; Joubert, D. From Ultrasoft Pseudopotentials to the Projector Augmented-Wave Method. *Phys. Rev. B: Condens. Matter Mater. Phys.* **1999**, *59*, 1758−1775.
(60) Slater, J. C. Statistical Exchange-Correlation in the Self-Consistent Field. *Adv. Quantum Chem.* **1972**, *6*, 1−92.
(61) Slater, J. C.; Johnson, K. H. Self-Consistent-Field X α Cluster Method for Polyatomic Molecules and Solids. *Phys. Rev. B: Solid State* **1972**, *5*, 844−853.
(62) Tao, S. X.; Cao, X.; Bobbert, P. A. Accurate and Efficient Band Gap Predictions of Metal Halide Perovskites Using the DFT-1/2 Method: GW Accuracy with DFT Expense. *Sci. Rep.* **2017**, *7*, 14386.
(63) Brivio, F.; Caetano, C.; Walsh, A. Thermodynamic Origin of Photoinstability in the $CH_3NH_3Pb(I_{1-x}Br_x)_3$ Hybrid Halide Perovskite Alloy. *J. Phys. Chem. Lett.* **2016**, *7*, 1083−1087.
(64) Sher, A.; van Schilfgaarde, M.; Chen, A.-B.; Chen, W. Quasichemical Approximation in Binary Alloys. *Phys. Rev. B: Condens. Matter Mater. Phys.* **1987**, *36*, 4279−4295.
(65) Grote, C.; Berger, R. F. Strain Tuning of Tin-Halide and Lead-Halide Perovskites: A First-Principles Atomic and Electronic Structure Study. *J. Phys. Chem. C* **2015**, *119*, 22832−22837.
(66) Thiele, G.; Serr, B. Crystal Structure of Rubidium Triiodostannate (II), $RbSnI_3$. *Z. Kristallog.—Cryst. Mater.* **1995**, *210*, 64.
(67) Scaife, D. E.; Weller, P. F.; Fisher, W. G. Crystal preparation and properties of cesium tin(II) trihalides. *J. Solid State Chem.* **1974**, *9*, 308−314.
(68) Lang, L.; Zhang, Y.-Y.; Xu, P.; Chen, S.; Xiang, H. J.; Gong, X. G. Three-Step Approach for Computing Band Offsets and Its Application to Inorganic ABX_3 Halide Perovskites. *Phys. Rev. B: Condens. Matter Mater. Phys.* **2015**, *92*, 075102.
(69) Krishnamoorthy, T.; Ding, H.; Yan, C.; Leong, W. L.; Baikie, T.; Zhang, Z.; Sherburne, M.; Li, S.; Asta, M.; Mathews, N.; et al. Lead-Free Germanium Iodide Perovskite Materials for Photovoltaic Applications. *J. Mater. Chem. A* **2015**, *3*, 23829−23832.
(70) Carignano, M. A.; Aravindh, S. A.; Roqan, I. S.; Even, J.; Katan, C. Critical Fluctuations and Anharmonicity in Lead Iodide Perovskites from Molecular Dynamics Supercell Simulations. *J. Phys. Chem. C* **2017**, *121*, 20729−20738.
(71) Zhou, X.; Jankowska, J.; Dong, H.; Prezhdo, O. V. Recent Theoretical Progress in the Development of Perovskite Photovoltaic Materials. *J. Energy Chem.* **2017**, *27*, 637.
(72) Ma, C.-G.; Krasnenko, V.; Brik, M. G. First-principles calculations of different (001) surface terminations of three cubic perovskites $CsCaBr_3$, $CsGeBr_3$, and $CsSnBr_3$. *J. Phys. Chem. Solids* **2018**, *115*, 289−299.
(73) Ju, M.-G.; Dai, J.; Ma, L.; Zeng, X. C. Lead-Free Mixed Tin and Germanium Perovskites for Photovoltaic Application. *J. Am. Chem. Soc.* **2017**, *139*, 8038−8043.
(74) Da Silva, E. L.; Skelton, J. M.; Parker, S. C.; Walsh, A. Phase Stability and Transformations in the Halide Perovskite $CsSnI_3$. *Phys. Rev. B: Condens. Matter Mater. Phys.* **2015**, *91*, 144107.
(75) Marshall, K. P.; Tao, S.; Walker, M.; Cook, D. S.; Lloyd-Hughes, J.; Varagnolo, S.; Wijesekara, A.; Walker, D.; Walton, R. I.; Hatton, R. A. $Cs_{1-x}Rb_xSnI_3$ Light Harvesting Semiconductors for Perovskite Photovoltaics. *Mater. Chem. Front.* **2018**, *2*, 1515−1522.
(76) Saliba, M.; Matsui, T.; Seo, J.-Y.; Domanski, K.; Correa-Baena, J.-P.; Nazeeruddin, M. K.; Zakeeruddin, S. M.; Tress, W.; Abate, A.; Hagfeldt, A.; Grätzel, M. Cesium-Containing Triple Cation Perovskite Solar Cells: Improved Stability, Reproducibility and High Efficiency. *Energy Environ. Sci.* **2016**, *9*, 1989−1997.
(77) Marshall, K. P.; Walker, M.; Walton, R. I.; Hatton, R. A. Elucidating the role of the hole-extracting electrode on the stability and efficiency of inverted $CsSnI_3/C_{60}$ perovskite photovoltaics. *J. Mater. Chem. A* **2017**, *5*, 21836−21845.
(78) Unger, E. L.; Kegelmann, L.; Suchan, K.; Sörell, D.; Korte, L.; Albrecht, S. Roadmap and Roadblocks for the Band Gap Tunability of Metal Halide Perovskites. *J. Mater. Chem. A* **2017**, *5*, 11401−11409.

DOI: 10.1021/acs.jpcc.8b04013
J. Phys. Chem. C 2018, 122, 17660−17667